Desalination and Water Treatment
www.deswater.com

doi: 10.1080/19443994.2016.1141374

57 (2016) 23827–23843
October

Taylor & Francis
Taylor & Francis Group

Modified *Camelorum* tree particles as a new adsorbent for adsorption of Hg(II) from aqueous solutions: kinetics, thermodynamics and non-linear isotherms

A. Hashem[a,b,*], Hamdy A. Hammad[c], A. Al-Anwar[d]

[a]*National Research Center, Textile Research Division, Cairo, Egypt, email: alihashem2000@yahoo.com*
[b]*Faculty of Science and Arts at Shaqra, Shaqra University, Shaqra, Saudi Arabia*
[c]*Faculty of Science, Chemistry Department, Al-Azhar University, Nasr City, Cairo, Egypt, email: dr.hamdyhammad@yahoo.com*
[d]*Assuit Laboratory, Medico-legal Department, Ministry of Justice, Assuit, Egypt, email: alaaelanwer@yahoo.com*

Received 27 May 2015; Accepted 26 December 2015

ABSTRACT

Camelorum tree (CT), a desert plant, has been utilized as an adsorbent material for the removal of Hg(II) ions from aqueous solution after treatment with malic acid at elevated temperature. Treated Camelorum tree (TCT) were found to exhibit excellent adsorption capacity over a wide range of Hg(II) concentration. Native CT and TCT were characterized by Fourier transform infrared spectroscopy and scanning electron microscopy to support the adsorption of Hg(II) ions. Effect of various parameters such as pH, adsorbent concentration, contact time, initial concentration, and temperature was investigated using batch process to optimize conditions for maximum adsorption. The adsorption data were analyzed using two, three, four, and five parameter models at 30˚C using nonlinear regression analysis. The maximum adsorption capacity (q_{max}) of Hg(II) onto TCT was 357.14 mg/g at an initial pH of 5 and a temperature of 30˚C. Thermodynamic parameters such as standard enthalpy change (ΔH°), free energy change (ΔG°), and entropy change (ΔS°) were also evaluated and the results indicated that adsorption of Hg(II) is spontaneous and exothermic. Various kinetics models including the pseudo-first-order, pseudo-second-order, intraparticle diffusion, Bangham, and Elovich models have been applied to the experimental data to predict the adsorption kinetics. Kinetic study was carried out by varying initial concentration of Hg(II) at constant temperature and it was found that pseudo-second-order rate equation was better obeyed than pseudo-first-order equation supporting that chemisorption process was involved. The examination of R^2 values and error analysis methods showed that the Langmuir–Freundlich, Dubinin–Radushkevich, Fritz–Schlunder (IV), and Fritz–Schlunder (V) models provide the best fit to experimental data than other isotherms and follow the following order: Langmuir–Freundlich (three parameter isotherm) > Dubinin–Radushkevich (two parameter isotherm) > Fritz–Schlunder (four parameter isotherm) > Fritz–Schlunder (five parameter isotherm). The obtained results show that TCT can be used as an effective and a low-cost adsorbent for the removal of Hg(II) from aqueous solutions.

Keywords: Camelorum tree; Malic acid; Hg(II) adsorption; Aqueous solution; Isotherm models; Adsorption kinetics; Thermodynamics

*Corresponding author.

1. Introduction

Industrial, agricultural, and domestic wastes pollute water bodies with heavy metals, which reach tissues through the food chain. The toxicity of heavy metals to aquatic organisms has been a subject of interest to biologist for many years. Among various types of pollution, the industrial waste constitutes the major source of various kinds of metal pollution in natural water. The highly toxic metals are Hg, Cd, Pb, Cu, and Cr which finds its way to the water bodies through wastewater from different industries as metal plating industries of cadmium, nickel, batteries, pigment, stabilizers, alloys, paint, metallurgical, tannery chemical manufacturing, mining, pulp and paper, oil refining, rubber processing, and fertilizers [1].

Mercury can be found in significant amounts in wastes from chloro-alkali manufacturing plants, electrical and electronics manufacturing, and sulfide ore roasting operations. Mercury is very harmful to humans, plants, and animals. Exposure to mercury can have toxic effects on reproduction, the central nervous system, liver, and kidney, and cause sensory and psychological impairments [2]. Therefore, all countries have taken measures to reduce mercury exposure through comprehensive prevention strategies including environmental standards that require removal of mercury from industrial effluents.

Various treatment technologies have been employed for the clean-up of waters contaminated with trace toxic metals in aquatic environments. Conventional techniques usually involve the application of physico-chemical processes such as precipitation, oxidation, reduction, solvent extraction, electrolytic extraction, dilution, electro-dialysis, filtration, flocculation, sedimentation, evaporation, osmosis, ion-exchange, chelation, biosorption, and adsorption [3].

Adsorption provides one of the most effective methods for removing heavy metal ions from aqueous solution [4]. Activated carbon is the most widely used adsorbent for this purpose because of its extended surface area, microporous structure, high adsorption capacity and high degree of surface reactivity. However, commercially activated carbons are very expensive [5]. This has led to a search for cheaper adsorbents. With this aim in mind, numerous low-cost alternative adsorbents have been proposed, including ligno-cellulosic wastes or polysaccharide biopolymers [6]. Agricultural byproducts mainly composed of cellulose and lignin which are available in large quantities and constitute one of the most abundant renewable resources in the world. Lignin has polar functional groups, which include alcohols, aldehydes, ketones, carboxylic, phenolic, and ether groups [7]. These groups have the ability to bind heavy metals by donation of an electron pair from these groups to form complexes with the metal ions in solution.

The adsorption capacity in general of crude agricultural byproducts is low. Chemical modification has shown great promise in improving the adsorption and the cation exchange capacity of agricultural byproducts [8]. Agricultural wastes have been examined for potential use as inexpensive adsorbents for heavy metal removal [9–15]. The abundant and availability of Camelorum tree (CT) particles as the desert plant makes them a good candidate for incorporation as precursor to prepare a new biosorbent for heavy metals from wastewater.

The main objective of this study was to investigate the feasibility of using TCT for the maximum removal of Hg(II) from aqueous solutions. The effect of such factors as pH, adsorbent dose, contact time, initial adsorbate concentration, and temperature was investigated. The kinetics of Hg(II) adsorption on the adsorbent was analyzed by fitting various kinetic adsorption isotherm models. The important of the adsorption isotherm models is to determine the best-fit isotherm equation in order to optimize the design of adsorption system for the removal of mercury utilizing TCT. Experimental equilibrium data were fitted to the Langmuir, Freundlich, Temkin, Dubinin and Halsey (two parameter isotherms), Redlich–Peterson, Toth, Sips, Khan and Hill, Radke–Prausnitz, and Langmuir–Freundlich (three parameter isotherms), Baudo and Fritz–Schlunder (four parameter isotherms and Fritz–Schlunder (five parameter isotherm) using nonlinear regression analysis. Error analysis was carried out to test the adequacy and the accuracy of the isotherm models. Thermodynamic parameters were evaluated and the adsorption was spontaneous and exothermic.

2. Experimental

2.1. Materials

CT, a desert plant, was obtained from the Martouh desert, Egypt. The roots were separated from the stems and leaves, washed with distilled water several times to remove the surface adhered particles and water soluble particles and dried at 80˚C in an electric oven for 24 h and ground using a mixer, and sieved to pass through a 50–150 μm. The roots were chosen because they contain the highest percentage of the cellulose content. The adsorbent was characterized by FT-IR spectroscopy and scanning electron microscopy (SEM).

2.2. Methods

2.2.1. Preparation of TCT adsorbent

TCT was prepared employing the following method. To a beaker containing 2 g of CT powder with particle sizes in the range of 50–150 μm was added to a known weight of malic acid (dissolved in the least amount of water) under continuous stirring with a spatula until a homogeneous paste was obtained. The paste was then transferred to a Pyrex Petri dish and placed in an air-circulated oven at 100–150˚C for a known length of time. The thermally treated sample was subsequently cooled to room temperature and ground. The soluble byproducts and any unreacted malic acid were removed by washing the sample several times with a water/ethanol (20:80) mixture for 2 h, with the final purified material being dried at 60˚C for 4 h.

2.2.2. Adsorption studies

A known volume (100 mL) of a Hg(II) ion solution with a concentration in the range of 100–1,000 mg L^{-1} was placed in a 125 mL Erlenmeyer flask. An accurately weighed sample of TCT adsorbent (0.05 g) with a particle size in the range 50–150 μm was then added to the solution. A series of such flasks was prepared, the pH values of the contents adjusted by the addition of 0.1 M HNO_3 or 0.1 M NaOH and then shaken at a constant speed of 150 rpm in a shaking water bath at 30˚C for a known time length. At the end of the agitation time, the metal ion solutions were separated by filtration. Blank experiments were carried out simultaneously without the addition of the TCT adsorbent. The extent of metal ion adsorption onto adsorbent was calculated mathematically by measuring the metal ion concentration before and after the adsorption through direct titration against the standard EDTA solution. The amount of Hg(II) adsorbed on TCT at equilibrium, q_e (mg/g) and percent removal of mercury were calculated according to the following relationships:

$$q_e = \frac{(C_0 - C_e)\,V(l)}{W} \tag{1}$$

$$\text{Percent removal} = \frac{(C_0 - C_e)}{C_0} \times 100\% \tag{2}$$

where C_0 and C_e are the initial and final concentrations of Hg(II), mg L^{-1}, V is the volume (L) of Hg(II), and W is the weight of TCT adsorbent (g). All adsorption experiments were carried out in duplicate and the mean values of q_e were reported.

2.3. Error analysis

In the single-component isotherm studies, the optimization procedure requires an error function to be defined to evaluate the fit of the isotherm to the experimental equilibrium data. The common error functions for determining the optimum isotherm parameters were, sum of absolute errors (EABS), Marquardt's percent standard deviation (MPSD), hybrid fractional error function (HYBRID), sum of the squares of the errors (ERRSQ), average percentage error (APE), and average relative error (ARE) [16]. In the present study, all error functions were used to determine the best fit in isotherm model as:

2.3.1. The sum of absolute error

$$\text{EABS} = \sum_{i=1}^{n} \left| (q_e)_{\text{exp.}} - (q_e)_{\text{calc.}} \right|_i \tag{3}$$

2.3.2. Marquardt's percent standard deviation

$$\text{MPSD} = 100 \sqrt{\frac{1}{n-p} \sum_{i=1}^{n} \left[\frac{((q_e)_{\text{exp.}} - (q_e)_{\text{calc.}})}{(q_e)_{\text{exp.}}} \right]^2} \tag{4}$$

2.3.3. Hybrid fraction error function (hybrid)

$$\text{Hybrid} = \frac{100}{n-p} \sum_{i=1}^{n} \left[\frac{((q_e)_{\text{exp.}} - (q_e)_{\text{calc.}})^2}{(q_e)_{\text{exp.}}} \right]_i \tag{5}$$

2.3.4. The Sum of the Squares of the Error (ERRSQ)

$$\text{ERRSQ} = \sum_{i=1}^{n} [(q_e)_{\text{calc.}} - (q_e)_{\text{exp.}}]^2 \tag{6}$$

2.3.5. Average percentage error

$$\text{APE } \% = \frac{\sum_{i=1}^{N} \left| [((q_e)_{\text{exp.}} - (q_e)_{\text{calc.}})/q_{\text{exp.}}] \right|}{N} \times 100 \tag{7}$$

2.3.6. Average relative error

$$\text{ARE} = \sum_{i=1}^{n} \left| \frac{(q_e)_{\text{exp.}} - (q_e)_{\text{calc.}}}{(q_e)_{\text{exp.}}} \right|_i \tag{8}$$

2.4. Analyses

2.4.1. FT-IR spectroscopy

The Fourier Transform infrared spectroscopy (FT-IR) was used to determine the vibrational frequencies of the functional groups in the adsorbents. The IR spectra were recorded on a Perkin–Elmer Spectrum 1000 spectrophotometer over 4,000–400 cm^{-1} using KBr disk technique.

2.4.2. Scanning electron microscopy

To carry out an SEM analysis, the sample was first mounted on a standard microscope stub and coating with a thin layer of gold using a Polaron Diode Sputter unit. The analysis was performed using a JEOL JSM 840 scanning electron microscope. The SEM was used to identify the surface quality and morphology of CT and TCT before and after Hg(II) adsorption.

2.4.3. Carboxyl content

The carboxyl contents of the native CT and TCT were determined according to the reported method [17].

3. Results and discussion

3.1. Characterization of adsorbent

3.1.1. FT-IR Studies

3.1.1.1. FT-IR Spectra. The FT-IR spectra of CT, TCT, and Hg(II)-loaded TCT are illustrated in Figs. 1(a)–(c), respectively. The difference in the fingerprint regions of the spectra are clear and confirm the modification and adsorption processes.

Fig. 1(a) shows a broadband at 3,420 cm^{-1}, characteristic of the hydroxyl group of CT cellulose. The bands at 2922.29 cm^{-1} in IR spectra of CT biomass may be due to the C–H stretching vibrations. The bands appearing at 1636.02 and 1379.64 cm^{-1} are attributed to the formation of oxygen functional groups like a highly conjugated C=O stretching in carboxylic groups. The peak appeared at 1057.83 cm^{-1} has been assigned to C–O stretching in ethers. The peak at 604.24 cm^{-1} is caused by C–N–C.

Fig. 1(b) shows the appearance of new peak at 1747.93 cm^{-1} characteristic of the carboxylic acid ester due to the formation of TCT after thermal treatment with malic acid. The FT-IR spectrum in Fig. 1(b) also exhibits broadening at 3428.46 cm^{-1} due to hydrogen bonding between the –OH group of the carboxylic acid and –OH groups in the cellulose chains of CT.

Fig. 1(c) shows small shift in the absorbance peak in Hg(II)-loaded TCT compared with that in CT and TCT (Fig. 1(a) and (b)). The broadband observed at 3428.46 cm^{-1} was shifted to 3420.63 cm^{-1}. The peaks at 2922.29 and 1733.67 cm^{-1} were shifted to 2921.33 and 1733.57 cm^{-1}, respectively. The peaks observed at 1636.02 and 1057.83 cm^{-1} were shifted to 1635.69 and 1058.66 cm^{-1}. Fig. 1(c) shows the appearance of new peaks at 1395.51 and 3565 cm^{-1} which can be attributed to the adsorbed mercury onto TCT. It should also be noted that the FTIR results did not provide any quantitative analysis as well as the information about the level of affinity to metal of the functional groups presented in the adsorbents. They only presented the possibility of the coupling between the metal species and the functional group of the adsorbents.

3.1.2. SEM studies

The surface morphology of the TC, TCT and Hg (II)-loaded TCT is shown in Fig. 2(a)–(c), respectively. SEM micrograph of CT and TCT (Fig. 2(a) and (b)) revealing the irregular nature of biomass particles, which is rough and heterogeneous with considerable amount of voids and lot of ups and downs. The adsorption of Hg(II) by TCT is demonstrated by the change in morphology in the surface of adsorbent (Fig. 2(c)). After Hg adsorption the tubes appear to be

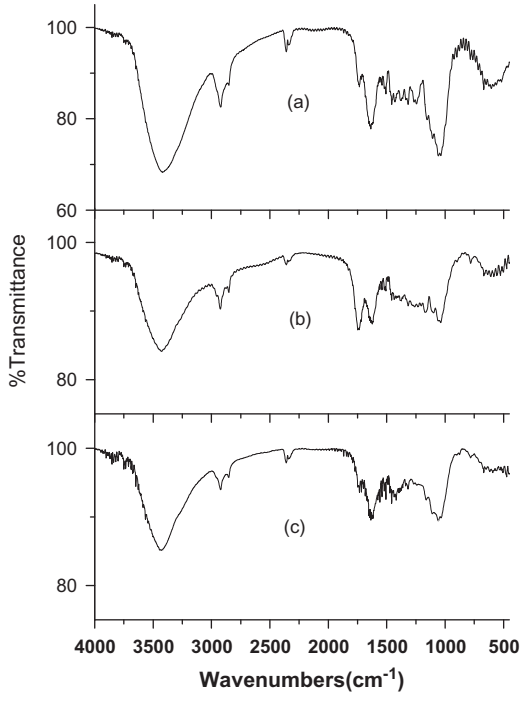

Fig. 1. FT-IR of CT (a), TCT (b), and Hg(II)-loaded TCT (c).

prominently swollen as Hg enters the pores of the TCT (Fig. 2(b)). This observation indicates that Hg is adsorbed to the functional groups present in the TCT structure. Based on the surface morphology results of TCT, it is suggested that the TCT can be used as adsorbent for liquid-solid adsorption processes.

3.2. Treatment of native CT with malic acid

Previous reports [18] have indicated that citric acid forms an anhydride when subjected to heat treatment. The presence of native CT particles with malic acid during the heating process would allow the anhydride to react with the cellulose hydroxyls of the native CT to form the TCT bearing carboxyl group. Further heating could result in further dehydration with the possibility of the cross-linked cellulose. Therefore, it is important to study the factors affecting the reaction between native CT and malic acid as shown below.

3.2.1. Effect of malic acid concentration

This effect shows the dependence of the extent of modification of CT on the concentration of malic acid. The data (figure not shown) show that the carboxyl group content increased significantly from 128 to 512 mequiv/100 g sample on increasing the concentration of malic acid from 1.86 to 14.92 mmol L^{-1}, and then remained at approximately the same level for higher malic acid concentrations. The increase in the carboxyl group content on increasing the malic acid concentration may be attributed to the greater availability of malic acid molecules in the proximity of the CT cellulose macromolecules. The latter were converted to the corresponding anhydride through dehydration under the effect of high temperature. The hydroxyl groups in the CT cellulose molecule are essentially the functional sites at which the reaction occurs. Since these groups are immobile, it is essential that there should be a greater availability of malic acid molecules in the vicinity of the cellulose hydroxyl groups if reaction is to occur. The anhydride obtained reacts with the cellulose hydroxyl groups of CT to form TCT.

3.2.2. Effect of reaction temperature

This effect shows the effect of temperature over the range of 100–150˚C on the extent of modification of CT with malic acid. The data (figure not shown) show that the carboxyl group content of CT increased from 165 to 509 mequiv/100 g sample on increasing the temperature from 100 to 140˚C, and then decrease for higher temperature in the range studied. This enhancement in carboxyl group content is a direct consequence of the favorable effect of temperature on (a) the swelling and accessibility of the cellulose component of CT, (b) the conversion of malic acid to malic acid anhydride, and (c) the mobility of malic acid anhydride molecules and their collision with the cellulose hydroxyl groups of CT to form TCT. The decrease in the carboxyl groups at temperature above 140˚C could be attributed to the catalytic effect of higher temperature on the reaction product. Reaction temperatures above 150˚C were not employed due to the conversion of the cellulosic material to ash.

3.2.3. Effect of dehydration time

This effect shows the extent of modification of CT when the latter was subjected to malic acid treatment at a fixed temperature (140˚C) for different time lengths. It is clear from the data (figure not shown) that the carboxyl group content of TCT increased significantly from 274.6 to 526 mequiv/100 g sample when the reaction time was increased from 30 to 150 min and then remained at approximately the same level for higher reaction time. The increase in the carboxyl group content by prolonged reaction is a direct consequence of the favorable effect of time on the formation of malic acid anhydride and the mobility of these molecules in their reaction with the cellulose hydroxyl groups of CT particles to form TCT.

3.2.4. Effect of adsorbent particle size range

Table 1 shows the effect of the particle size range on the extent of modification of CT. It is clear that, within the range examined (50–350 μm), the smaller the CT size range, the greater the carboxyl group content of the resulting TCT. The enhancement in the carboxyl group content could be interpreted in terms of the larger surface area of smaller particles being available for modification.

3.3. Factors affecting adsorption of Hg(II) onto TCT

3.3.1. Effect of pH of adsorbate

The pH of the aqueous solution containing metal ions is an important parameter in adsorption processes [19]. The data (figure not shown) shows the effect of pH on the adsorption capacity of TCT towards Hg(II) ions over the pH range 2.0–6 at a fixed initial metal ion concentration of 300 mg/l. It is clear from this data that the adsorption capacity increased from 9.5 to 306 mg/g on increasing the pH of the adsorbate from 2.0 to 5.0 and then decreased with

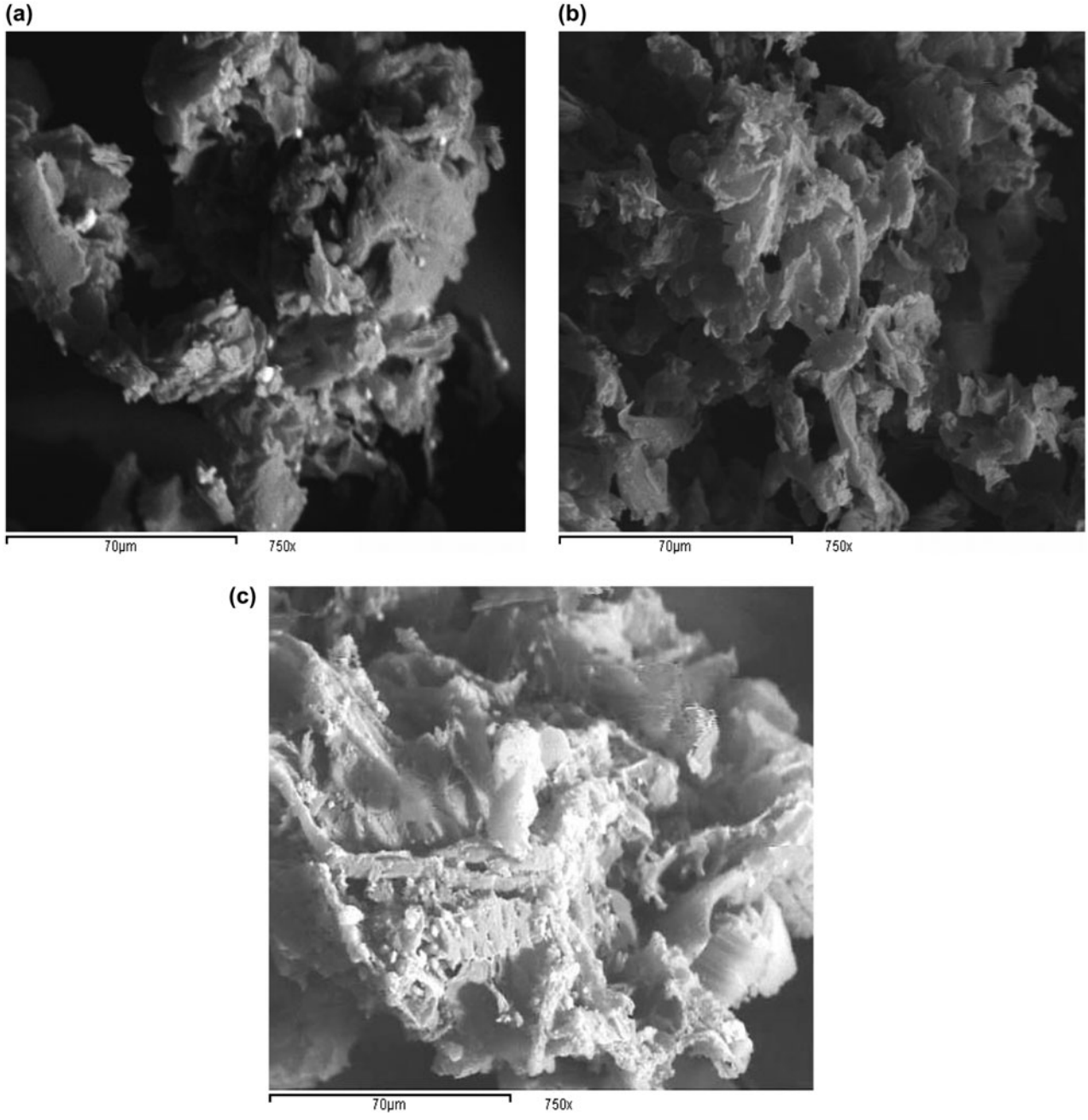

Fig. 2. SEM of CT (a), TCT (b), and Hg(II)-loaded TCT (c).

further increase of pH within the range studied. The adsorption of Hg(II) ions onto the surface of TCT occurs via an ion-exchange mechanism as shown in Eqs. (9) and (10):

$$2TCT - COOH \Leftrightarrow 2TCT - COO^- + 2H^+ \quad (9)$$

$$2TCT - COO^- + M^{2+} \Leftrightarrow (TCT - COO)_2M \quad (10)$$

where M^{2+} denotes the metal ion. Eq. (9) represents deprotonation, which is the first stage in ion exchange, while Eq. (10) represents the attachment or adsorption of the metal cation onto the deprotonated surface. It is clear from Fig. 6 that the adsorption capacity, q_e, of TCT towards Hg(II) ions was 9.5 mg/g at pH 2. This is because the high concentration of H^+ ions present in the solution at this pH shifts the equilibrium

Table 1
Effect of particle size on the carboxyl group content of TCT

Particle size range (μm)	Carboxyl group content (m eq/100 g sample)
50–150	479.064
150–250	447.0443
250–350	409.4827

depicted in Eq. (9) mainly to the left. This implies that the active –COOH groups are not ionized and, hence, the ion-exchange sites on the TCT surface are still protonated. The increase in the adsorption capacity, q_e, brought about by increasing the pH value up to 5 could be attributed to the ion-exchange sites becoming increasingly ionized and the metal ions becoming adsorbed according to Eq. (10). The decrease in the adsorption capacity above pH 5 could be attributed to the decrease in the positive charge of the Hg(II) species. Adsorption studies could not be carried out at pH values above 6 because of the conversion of Hg(II) ions to mercuric hydroxide.

3.3.2. Effect of adsorbent concentration

The effect of adsorbent dose on both the adsorption capacity and the percentage removal of Hg(II) ions onto TCT were studied at pH 5 employing adsorbent doses within the range 0.5–8 g/land at a fixed initial metal ion concentration of 300 mg L^{-1}. It is apparent from the corresponding data depicted in Fig. 3 that the percentage removal of Hg(II) ions increased with the increasing adsorbent dosage, which may be due to the increase in the surface area of the adsorbent and the availability of more adsorption sites. On the other hand, the adsorption capacity (q_e) or the amount of Hg(II) ions adsorbed per unit mass of adsorbent decreased with increasing adsorbent dosage. This behavior may be mainly due to overlapping of the adsorption sites as a result of the overcrowding of adsorbent particles in the system and also to the competition among Hg(II) ions for surface sites [20].

3.3.3. Effect of contact time

Fig. 4 shows the effect of agitation time at various initial adsorbate concentrations on the adsorption capacity of TCT towards Hg(II) ions. It will be seen that the adsorption capacity increased with increasing agitation time and initial concentration of the adsorbate, remaining virtually constant after equilibrium had been attained. The time necessary to achieve equilibrium increased with increasing adsorbate concentration, being 30, 45, and 60 min for adsorbate concentrations of 310, 405, and 607 mg L^{-1}, respectively. This contact time, which is one of the parameters for economical wastewater treatment plant operations, is quite small.

3.3.3.1. Adsorption kinetics. In order to examine the controlling mechanism of adsorption process such as mass transfer and chemical reaction, kinetic models were used to test experimental data. Many applications, such as wastewater treatment and metal ions removal need a rapid adsorption rate and short contact time. The kinetic models were

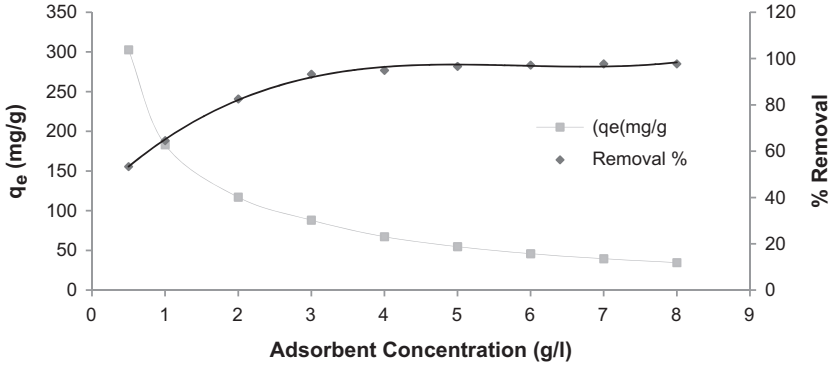

Fig. 3. Effect of adsorbent concentration on adsorption capacity and percentage removal of Hg(II) onto TCT at 30˚C. Notes: Reaction Conditions: particle size, 125 μm; adsorbate concentration, 300 mg L^{-1}; pH 5; contact time, 2 h; carboxyl content, 490.6 m eq/100 g sample, and adsorption temperature, 30˚C.

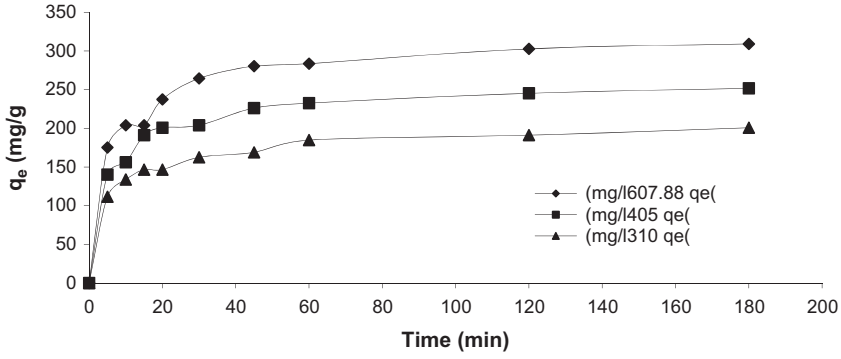

Fig. 4. Effect of agitation time on adsorption capacity of Hg(II) ions onto TCT at 30˚C.
Notes: Reaction Conditions: particle size, 125 μm; pH 5; carboxyl content, 490.6 m eq/100 g sample and adsorption temperature, 30˚C.

pseudo-first-order, pseudo-second-order, intraparticle diffusion, Bangham's equation, and Elovich model which are expressed as follows:

The pseudo-first-order model [21] is represented as:

$$\log(q_e - q_t) = \log q_e - \frac{k_1.t}{2.303} \tag{11}$$

The pseudo-second-order model [22] is represented as:

$$\frac{t}{q_t} = \frac{1}{(k_2 \cdot q_e^2)} + \frac{t}{q_e} \tag{12}$$

The intraparticle diffusion model [23] can be expressed by the following equation:

$$q_t = k_P.t^{\frac{1}{2}} + C \tag{13}$$

where k_1 is the pseudo-first-order rate constant (mg g^{-1} min^{-1}); k_2 is the pseudo-second-order rate constant (g mg^{-1} min^{-1}); k_P is the intraparticle diffusion rate constant (mg g^{-1} $min^{-1/2}$), C is the thickness of the boundary layer (mm); and q_e is the amount of adsorbate adsorbed at equilibrium (mg g^{-1}), while q_t is the amount of adsorbate adsorbed at time t (mg g^{-1}) before reaching equilibrium.

Bangham's equation [24] was employed for applicability of adsorption of Hg(II) onto TCT. Bangham's equation was used to evaluate whether the adsorption is pore-diffusion controlled.

$$\log \log\left(\frac{C_o}{C_o - q_m}\right) = \log\left(\frac{k_o m}{2.303}\right) + \alpha \log t \tag{14}$$

where, C_o is the initial concentration of the adsorbate (mg L^{-1}), V is the volume of the adsorbate (mL), m is the weight of adsorbent (g L^{-1}), q (mg g^{-1}) is the amount of adsorbate retained at time t, and α (<1) and k_o are the constants.

The Elovich model equation [25] is generally expressed as:

$$q_t = \frac{1}{\beta}\ln(\alpha\beta) + \frac{1}{\beta}\ln(t) \tag{15}$$

where α (mg g^{-1} min^{-1}) is the initial adsorption rate and the parameter β (g mg^{-1} L) is related to the extent of surface coverage and activation energy for chemisorption.

Pseudo-first-order model is rendered the rate of occupation of the adsorption sites to be proportional to the number of unoccupied sites. A pseudo-first-order kinetic process (Eq. (11)) is usually considered physical adsorption and the whole process is diffusion controlled. The slopes and intercepts of plots of log ($q_e - q_t$) vs. t for the concentrations of 310, 405, and 607 mg L^{-1} were used to determine the pseudo-first-order constant and equilibrium adsorption density, q_e. However, the q_e of experimental data deviated considerably from the theoretical data from the pseudo-first-order model (Table 2). A comparison of the results with the correlation coefficients is shown in Table 2. The correlation coefficients for the pseudo-first-order kinetic model obtained for concentrations of 310, 405, and 607 mg L^{-1} were low (figure not shown). This suggests that this adsorption of Hg(II) onto TCT is not acceptable for pseudo-first-order reaction.

Pseudo-second-order kinetic model (Eq. (12)) is assumed the chemical reaction mechanisms [26]

Table 2
Kinetic parameters for adsorption of Hg(II) onto TCT at 30°C

Models	Parameters	Values (310 mg/l)	(405 mg/l)	(607 mg/l)
Pseudo-first-order	k_1	0.001842	0.002994	0.005272
	R^2	0.7745	0.7166	0.763
	$q_{e(exp.)}$	191.208	245.3836	302.746
	$q_{e(calc.)}$	246.49	206.68	168.42
Pseudo-second-order	K_2	0.000715	0.000639	0.0005455
	$q_{e(exp.)}$	191.208	245.3836	302.746
	$q_{e(calc.)}$	204.0816	256.4103	322.58
	R^2	0.9988	0.9996	0.996
Bangham's equation	K_0	0.36983	0.572646	0.372203
	α	0.184	0.19	0.1867
	R^2	0.9649	0.9213	0.9312
Intra-Particle diffusion	K_P	10.406	14.66	19.694
	C	102.69	125.01	142.46
	R^2	0.9727	0.8748	0.9036
Elovich equation	α	538.3083473	614.7283296	668.0538
	β	0.040530134	0.031080997	0.024849
	R^2	0.9803	0.9482	0.9474

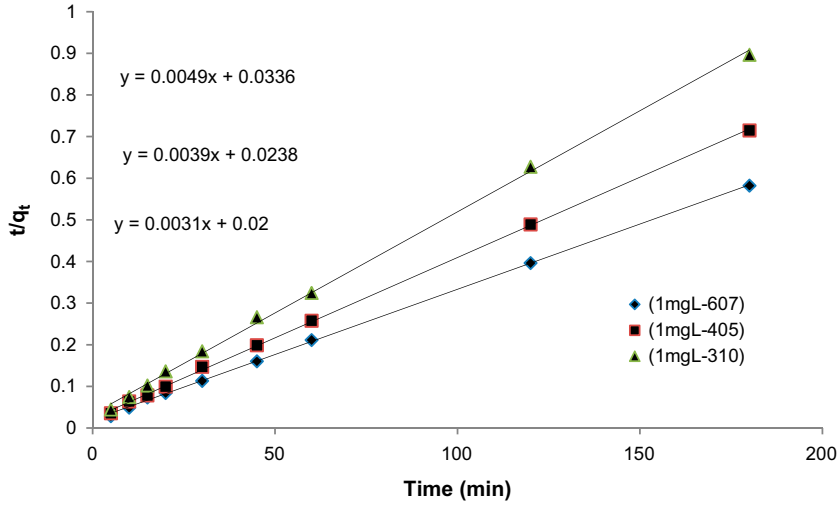

Fig. 5. Pseudo-second-order reaction of Hg(II) onto TCT at concentrations of 310, 405, and 607 mg L^{-1}.

and the biosorption rate is controlled by chemical biosorption through sharing or exchange of electrons between the adsorbate and adsorbent. Therefore, the adsorption behavior belonging to the pseudo-second-order kinetic model is a chemical process.

The slopes and intercepts of plots t/q_t vs. t were used to calculate the pseudo-second-order rate constants k_2 and q_e. The straight lines in plots of t/q vs. t Fig. 5 show good agreement of experimental data with the pseudo-second-order kinetic model for concentrations of 310, 405, and 607 mg L^{-1}. Table 2 lists the computed results obtained from the pseudo-second-order kinetic model. The correlation coefficients for pseudo-second-order kinetic model obtained were greater than 0.99 for the three concentrations used. The calculated q_e values also agree very well with the experimental data (Table 2). This indicates that the adsorption of Hg(II) onto TCT is acceptable for this model.

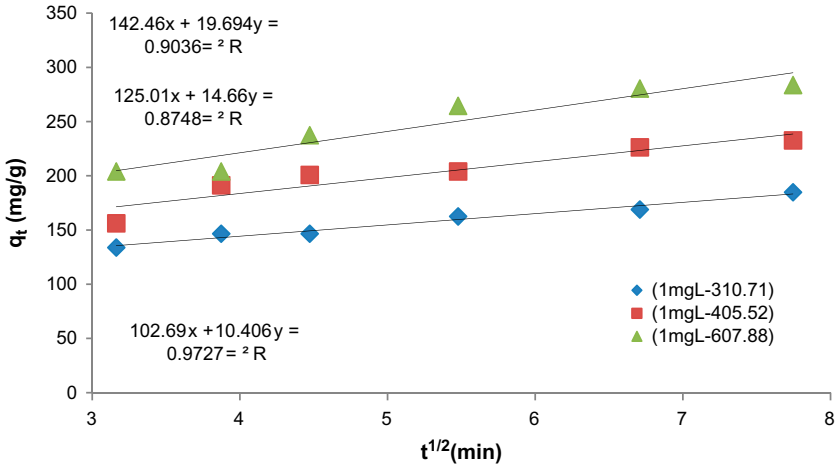

Fig. 6. Test-intraparticle diffusion of Hg(II) onto TCT at concentrations of 310, 405, and 607 mg L^{-1}.

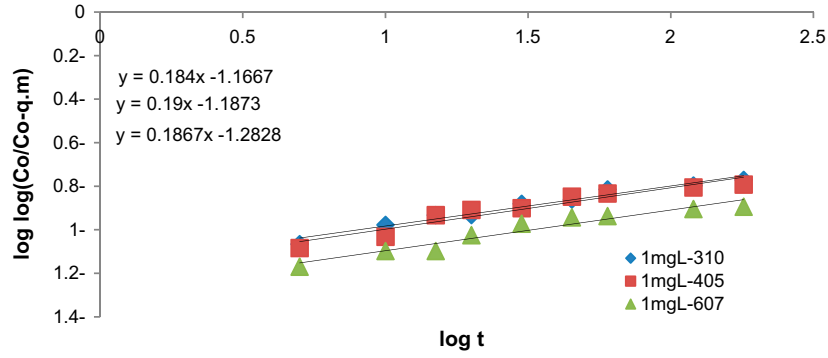

Fig. 7. Bangham's model of Hg(II) onto TCT at concentrations of 310, 405, and 607 mg L^{-1}.

The pseudo-first-order and pseudo-second-order kinetic models cannot describe the diffusion mechanism, thus kinetic results need to be evaluated by using the intraparticle diffusion model as given in Eq. (13).

Adsorption process incorporates the transport of adsorbate from the bulk solution to the interior surface of the pores in TCT. The rate parameter for intraparticle diffusion, k_p for the Hg(II) on TCT is measured according to Eq. (13). The plots of q_t vs. $t^{1/2}$ for the adsorption of Hg(II) on TCT at different concentrations used (figure not shown). Different previous studied indicated that the plots of q_t vs. $t^{1/2}$ were multi-linear two or more steps govern the adsorption process [27,28]. The plot is curved at the initial portion followed by linear portion and plateau. The initial curved portion is attributed to the bulk diffusion and the linear portion to the intraparticle diffusion, while the plateau corresponding to equilibrium.

The data of solid phase metal concentration against time t at the initial concentrations of 310, 405, and 607 mg L^{-1} of Hg(II) were further processed for testing the rate of diffusion in the adsorption process.

The slopes and intercepts of plots q_t vs. $t^{1/2}$ were used to calculate the intraparticle diffusion rate constant k_P (Fig. 6). The straight lines in plots of q_t vs. $t^{1/2}$ (Fig. 6) show good agreement of experimental data with the intraparticle diffusion model for concentrations of 310, 405, and 607 mg L^{-1}.

The deviation of straight line from the origin (Fig. 6) indicates that the pore diffusion is not the rate-controlling step [29]. The values of k_P

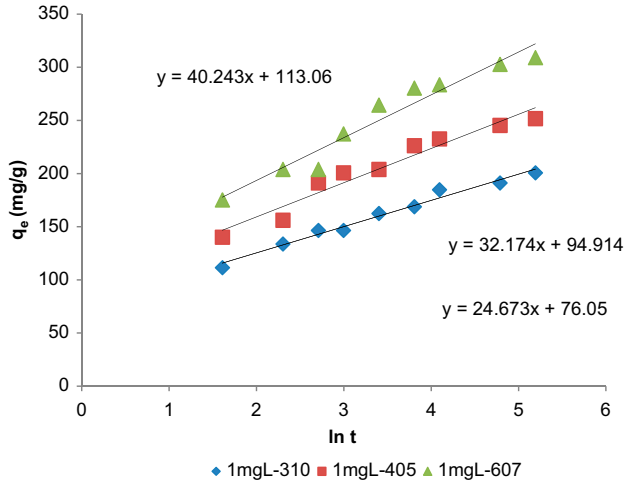

Fig. 8. Elovich model of Hg(II) onto TCT at concentrations of 310, 405, and 607 mg L^{-1}.

(mg g^{-1} min^{-1}) obtained from the slope of the straight line (Fig. 6) are listed in Table 2. The values of R^2 for the plots are also listed in Table 2. The values of intercept C (Table 2) give an idea about the boundary layer thickness, i.e. the larger the intercept, is the greater the boundary layer effect [30]. This value indicates that the adsorption of Hg(II) onto TCT is acceptable for intraparticle diffusion mechanism.

The plot of $\log\log(C_o/C_o - q_m)$ against log t as shown in Fig. 7 for the concentrations of 310, 405, and 607 mg L^{-1}. The plots were found to be linear for each concentration with good correlation coefficient (>0.92) for three concentrations indicating that kinetics confirmed to Bangham's equation and therefore the adsorption of Hg(II) onto TCT was pore diffusion controlled. The values of R^2 and the constants are listed in Table 2.

If Hg(II) adsorption onto TCT fits the Elovich model, a plot of q_t vs. ln t should yield a linear relationship with a slope of $(1/\beta)$ and an intercept of $(1/\beta)$ ln $(\alpha\beta)$.The straight lines in plots of q_t vs. ln t (Fig. 8) show good agreement of experimental data with the Elovich model for concentrations of 310, 405, and 607 mg L^{-1} ($R^2 > 0.94$). This suggests that the adsorption of Hg(II) onto TCT is acceptable for this system. The values of R^2 and the constants are also listed in Table 2.

3.3.4. Effect of temperature

The effect of temperature on the adsorption capacity of Hg(II) ions onto TCT was studied at pH 5 employing adsorbent dose of 0.5 g L^{-1} under different temperatures at 30, 40, and 50°C (figure not shown).

Table 3
Thermodynamic parameters for the adsorption of Hg(II) ions onto TCT at different temperatures

Temperature (K)	ΔG° (kJ mol^{-1})	ΔH° (kJ mol^{-1})	ΔS° (JK^{-1} mol^{-1})
303	6.57	100.6	296
313	7.94		
323	9.64		

Table 4
Comparison of sorption capacities of various adsorbents for Hg(II)

Adsorbents	Adsorption capacity (mg/g)	Refs.
Chemically modified peanut hull	83.3	[32]
Chemically treated sawdust (*Acacia arabica*)	20.62	[1]
Polyacrylamide grafted coconut coir pith	254.5	[33]
Treated walnut shell (WS)	151.5	[34]
Rice husk RH-NaOH	82.64	[35]
Waste brick	87	[36]
Carica papaya	155.63	[37]
Activated carbon prepared from palm oil empty fruit bunches	52.67	[38]
Activated carbon obtained from furfural	174	[39]
Carboxymethylated granular activated carbon	19.72	[40]
Malic acid treated CT	357.14	This study

Table 5
Lists of adsorption isotherm models

Isotherm	Equation (nonlinear form)	Refs.
Two parameter models		
Langmuir	$q_e = \frac{k_L.C_e}{1+a_L.C_e}$	[41]
Freundlich	$q_e = K_F.C_e^{1/n}$	[42]
Tempkin	$q_e = \frac{RT}{b_T}\ln(A_T C_e)$	[43]
Dubinin–Radushkevich	$q_e = q_D.\exp(-\beta_D\left[\mathrm{RT}\ln\left(1+\frac{1}{C_e}\right)\right]^2$	[44]
Halsey	$q_e = \exp\left(\frac{\ln k_H - \ln C_e}{n}\right)$	[45]
Three parameter models		
Redlich-Peterson	$q_e = \frac{A.C_e}{1+B.C_e^g}$	[46]
Toth	$q_e = \frac{k_t.C_e}{(a_t+C_e)^{1/t}}$	[47]
Sips	$q_e = \frac{k_s.C_{es}^B}{1+a_s.C_{es}^B}$	[48]
Khan	$q_e = \frac{q_k.b_K.C_e}{(1+b_K.C_e)^{a_K}}$	[49]
Radke–Prausnitz	$q_e = \frac{\alpha_R.r_R.C_e^{\beta R}}{\alpha_R+r_R.C_e^{\beta R-1}}$	[50]
Langmuir–Freundlich	$q_e = \frac{q_{mLF}.(k_{LF}.C_e)^{mLF}}{1+(k_{LF}.C_e)^{mLF}}$	[51]
Hill	$q_e = \frac{q_{sH}.C_e^{nH}}{k_D+C_e^{nH}}$	[52]
Four parameter models		
Baudo	$q_e = \frac{qmo.bo.C_e^{(1+x+y)}}{1+bo}$	[53]
Fritz–Schlunder	$q_e = \frac{A.C_e^1}{1+B.C_e^\beta}$	[54]
Five parameter models		
Fritz–Schlunder	$q_e = \frac{q_{mFS}.k_1.C_e^{m_1}}{1+k_2.C_e^{m_2}}$	[54]

The data indicate that the adsorption capacity increase with increasing the temperature from 30 to 50°C. This is showed that adsorption process has been affected by temperature rise.

3.3.4.1. Thermodynamic parameters. The original concepts of thermodynamics assume that in an isolated system, where energy cannot be gained or lost, the entropy change is the driving force. In environmental engineering practice, both energy and entropy factors must be taken into account in determining what processes will occur spontaneously. Thermodynamic parameters such as the standard free energy (ΔG°), the enthalpy change (ΔH°), and the entropy change (ΔS°) have been calculated for the present system using the following equations [31]. The standard free energy change (ΔG°) was calculated from Eq. (16):

$$\Delta G^\circ = -RT\ln a_L \tag{16}$$

where a_L is the Langmuir constant (L mg^{-1}), R is the universal gas constant (8.31441 JK^{-1} mol^{-1}) and T (K) is the absolute temperature. The equilibrium constant, a_L can be used via the Van't Hoff equation to determine the enthalpy change, ΔH° of adsorption as a function of temperature:

$$\ln\left(\frac{a_{L2}}{a_{L1}}\right) = \frac{\Delta H^\circ}{R}.\frac{(T_2-T_1)}{T_1.T_2} \tag{17}$$

where a_{L1}, a_{L2}, and $a_{L3}$are the Langmuir constants at 30, 40, and 50°C (303, 313, and 323 K), respectively. The positive values of ΔG° (Table 3) indicate the nonspontaneous nature of the adsorption of Hg(II) ions onto TCT. The positive values of ΔH° in the range of 30–50°C (303–323 K) listed in Table 3 suggest that the adsorption process was endothermic cover this temperature range. The entropy change (ΔS°) was calculated from Eq. (18):

Table 6
Constants and error analysis of two parameter models for adsorption of Hg(II) onto TCT at 30°C

Isotherm model	Parameter	Value	Error analysis	Value
Langmuir	a_L	0.013038175	ARE	0.447486239
			APE%	5.593577987
	k_L	5.557053359	EABS	98.69311314
			ERRSQ	2642.104101
	R^2	0.9827	Hybrid	234.8422784
			MPSD	0.958292638
Freundlich	$1/n$	0.211716386	ARE	0.840045824
			APE%	10.5005728
	K_F	93.70489057	EABS	177.2646739
			ERRSQ	8532.066323
	R^2	0.938	Hybrid	801.3593314
			MPSD	0.970396527
Tempkin	A_T	0.152625495	ARE	0.616239629
			APE%	7.702995362
			EABS	145.1033253
			ERRSQ	4748.7782
	R^2	0.9758	Hybrid	379.5340594
			MPSD	0.962206667
Dubinin–Radushkevich	q_D	356.6637935	ARE	0.221312665
			APE%	2.766408316
	B_D	5.806622278	EABS	52.52892244
			ERRSQ	596.0780796
	R^2	0.987	Hybrid	44.17294144
			MPSD	0.940632223
Halsey	K_H	94.09515865	ARE	0.840773989
			APE%	10.50967487
			EABS	177.2705751
			ERRSQ	8589.922848
	R^2	0.9379	Hybrid	805.6109662
			MPSD	0.970439629

$$\Delta G = \Delta H - T\Delta S \quad (18)$$

The positive values of ΔS° in the range of 30–50°C (303–323 K) shows the increase in randomness at the solid/solution interface during the adsorption of Hg (II) ions onto TCT.

3.3.5. Effect of adsorbate concentration (Adsorption isotherm)

Adsorption isotherm describe how adsorbates interact with adsorbents are critical in optimizing the use of adsorbents. The amount of adsorbate per unit mass of adsorbent at equilibrium, q_e (mg/g) and the adsorbate equilibrium concentration, C_e (mg L^{-1}) allows plotting the adsorption isotherm, q_e vs. C_e (figure not shown) at 30°C. The adsorption capacity of Hg (II) onto TCT was found to be 357.14 mg/g.

In comparison with other adsorbents reported in the literature for adsorption of mercury, the TCT had a good affinity for removal of mercury as shown in Table 4 [32–40].

Mathematical models can be used to describe and characterize the adsorption process. The most common isotherms for describing solid–liquid sorption systems are Langmuir, Freundlich, Temkin, Dubinin, and Halsey (two parameter isotherms), Redlich–Peterson, Toth, Sips, Khan, Hill, Radke–Prausnitz, and Langmuir–Freundlich (three parameter isotherms), Baudo and Fritz–Schlunder (four parameter isotherms), and Fritz–Schlunder (five parameter isotherm). Therefore, in order to investigate the adsorption capacity of Hg (II) onto TCT, the experimental data were fitted to these equilibrium models.

The equations of all adsorption isotherms [41–54] addressed in this paper are listed in Table 5.

The comparison between the experimental data and the data obtained from two, three, four, and five

Table 7
Constants and error analysis of three parameter models for adsorption of Hg(II) onto TCT at 30℃

Isotherm Model	Parameter	Value	Error analysis	Value
Redlich–Peterson	A	51.61557339	ARE	0.801271694
	B	0.479923596	APE%	10.01589617
			EABS	169.4405047
	g	0.807983735	ERRSQ	7721.82925
			Hybrid	871.2198001
	R^2	0.9437	MPSD	0.971215228
Toth	K_t	61.20680361	ARE	0.778463456
	a_T	0.301349296	APE%	9.730793194
			EABS	183.4273724
	$1/t$	0.702737506	ERRSQ	7354.81118
			Hybrid	704.5222341
	R^2	0.9659	MPSD	0.968167951
Sips	K_s	5.67238359	ARE	0.453497911
	a_s	0.013339532	APE%	5.668723891
			EABS	98.90720765
	β_s	0.998335718	ERRSQ	2715.732343
			Hybrid	294.1334039
	R^2	0.9821	MPSD	0.96054225
Khan	q_k	169.6923329	ARE	0.686872464
	a_k	0.775225085	APE%	8.585905803
			EABS	160.6521265
	b_k	0.070980595	ERRSQ	4988.601629
			Hybrid	513.3011595
	R^2	0.9679	MPSD	0.965553188
Hill	q_{SH}	376.2267559	ARE	0.224998521
	K_D	896.6063807	APE%	2.81248151
			EABS	51.99316845
	n_H	1.595037933	ERRSQ	637.7754462
			Hybrid	59.55736422
	R^2	0.9932	MPSD	0.944273307
Langmuir–Freundlich	q_{mLF}	360.4203	ARE	0.111873897
	K_{LF}	0.0137842	APE%	1.398423712
	m_{LF}	1.9881158	EABS	32.39851202
			ERRSQ	266.0311982
	R^2	0.9947	Hybrid	19.49631351
			MPSD	0.930465562
Radke–Prausnitz	α_R	5.921395465	ARE	0.474209174
	r_R	376.8579721	APE%	5.927614679
			EABS	103.9631531
	β_R	0.018709117	ERRSQ	2935.862179
			Hybrid	315.8369241
	R^2	0.9811	MPSD	0.96118677

parameter models (figures not shown) as well as the constants and error analysis of two, three, four, and five parameter models are given in Tables 6–9.

3.3.5.1. Error analysis and nonlinear regression method. The nonlinearized form of the different isotherm models are listed in Tables 6–9. For non-linear method, a trial and error procedure, which is applicable to computer operation is developed using solver add-in, Microsoft Excel. In the experimental and the predicted isotherms (figures not shown) by nonlinear method for the adsorption of Hg(II) onto TCT, the R^2 value is used to minimize the error distribution between the experimental equilibrium data and the predicted isotherms. The calculated isotherm parameters and their corresponding coefficient of determination, error analysis of the parameters and R^2 values were listed in Tables 6–9.

Table 8
Constants and error analysis of four parameter models for adsorption of Hg(II) onto TCT at 30˚C

Isotherm model	Parameter	Value	Error analysis	Value
Baudo	q_{m0}	505.79455	ARE	0.839433
			APE%	10.49292
	b_o	0.2260475	EABS	177.3013
			ERRSQ	8464.062
	x	−0.879136	Hybrid	1194.839
			MPSD	0.974292
	y	0.0918733		
	R^2	0.9386		
Fritz–Schlunder	A	288.33191	ARE	0.398314
			APE%	4.978923
	α	0.050228	EABS	88.57202
			ERRSQ	2164.081
	B	147.22059	Hybrid	281.9562
			MPSD	0.95991
	β	−1.23369		
	R^2	0.9854		

Table 9
Constants and error analysis of five parameter models for adsorption of Hg(II) onto TCT at 30˚C

Isotherm model	Parameter	Value	Error analysis	Value
Fritz–Schlunder	q_{mFS}	23.301401	ARE	0.811332
			APE%	10.14165
	K_1	23.301401	EABS	170.9849
			ERRSQ	7942.228
	K_2	6.0461306	Hybrid	1498.659
			MPSD	0.976517
	m_1	0.0601751		
	m_2	−0.252733		
	R^2	0.942		

Among two, three, four, and five parameter models, the highest R^2 value and lowest ARE, APE%, EABS, ERRSQ, MPSD, and Hybrid indicated that Langmuir–Freundlich (three parameter isotherm, Dubinin–Readushkevich (two parameter isotherm), Fritz–Schlunder (four parameter isotherm, and Fritz–Schlunder (five parameter isotherm) are the better fit than the rest of isotherm models. The acceptable models for the experimental data follow the following order:

Langmuir–Freundlich (three parameter isotherm) > Dubinin–Readushkevich (two parameter isotherm) > Fritz–Schlunder (four parameter isotherm > Fritz–Schlunder (five parameter isotherm).

4. Conclusions

CT particles were modified by treatment with malic acid at elevated temperatures to obtain TCT. Factors affecting the esterification of CT were investigated. These factors were malic acid concentration, reaction temperature, reaction time and particle size of the adsorbent. The CT and TCT samples were characterized by FT-IR spectral analysis and SEM before and

after adsorption of Hg(II). The carboxyl content of CT and TCT were also determined.

The TCT were utilized for the removal of Hg(II) ions from aqueous solution by using batch adsorption procedure. The results indicated that the adsorption capacity of TCT towards Hg(II) ions was affected by the pH, adsorbent concentration, agitation time, initial metal ion concentration, and temperature.

The data of the adsorption isotherm was tested by the Langmuir, Freundlich, Temkin, Dubinin–Radushkevich and Halsey (two parameter models), Redlich-Peterson, Toth, Sips, Khan, Radke–Prausnitz and Langmuir–Freundlich (three parameter models), Baudo and Fritz–Schlunder (four parameter models) and Fritz–Schlunder (five parameter models) using non-linear regression technique at 30˚C. The results obtained showed that the maximum adsorption capacity according to the Langmuir equation was 357.14 mg/g at 30˚C. The kinetics of adsorption of Hg(II) onto TCT have been discussed using five kinetic models, i.e. the pseudo-first-order model, the pseudo-second-order model, the Elovich equation, the intraparticle diffusion model, and Bangham equation. The adsorption of Hg(II) onto TCT could be well described by the pseudo-second-order kinetic model.

The best fitting model was firstly evaluated using six different error functions. The examination of all these error estimation methods showed that the Langmuir–Freundlich and Dubinin–Radushkevich models provide the best fit for experimental data than other isotherms. Thermodynamic studies indicated that the adsorption process was non-spontaneous and an endothermic reaction.

References

[1] A.K. Meena, K. Kadirvelu, G.K. Mishra, C. Rajagopal, P.N. Nagar, Adsorptive removal of heavy metals from aqueous solution by treated sawdust (Acacia arabica), J. Hazard. Mater. 150 (2008) 604–611.

[2] A. Hashem, Kh.A. Alkheraije, Chemically modified cornulaca monacantha biomass for bioadsorption of Hg(II) from contaminated water: Adsorption Mechanism, J. Environ. Prot. 4 (2013) 280–289.

[3] J.S. Kwon, S.T. Yun, J.H. Lee, S.O. Kim, H.Y. Jo, Removal of divalent heavy metals (Cd, Cu, Pb, and Zn) and arsenic(III) from aqueous solutions using scoria: Kinetics and equilibria of sorption, J. Hazard. Mater. 174 (2010) 307–313.

[4] M.M. Nassar, M.S. El-Geundi, Comparative cost of color removal from textile effluents using natural adsorbents, J. Chem. Technol. Biotechnol. 50 (1991) 257–264.

[5] G. McKay, Adsorption of dyestuff from aqueous solution with activated carbon: I. Equilibrium and batch contact time studies, J. Chem. Technol. Biotechnol. 32 (1982) 759–772.

[6] A. Hashem, F. Ahmad, R. Fahad, Application of some starch hydrogels for removal of Hg(II) from aqueous solutions, Adsorpt. Sci. Technol. 26 (2008) 563–579.

[7] A. Hashem, R. Akasha, A. Ghith, D.A. Hussein, Adsorbent based on agricultural wastes for heavy metal and dye removal: A review, Energy Educ. Sci. Technol. 19 (2007) 69–86.

[8] P.S. Keng, S.L. Lee, S.T. Ha, Y.T. Hung, S.T. Ong, Removal of hazardous heavy metals from aqueous environment by low-cost adsorption materials, Environ. Chem. Lett. 12 (2014) 15–25.

[9] S. Choudhary, S. Singh, V. Goyal, Removal of copper (II) and chromium (VI) from aqueous solution using sorghum roots (S. bicolor): A kinetic and thermodynamic study, Clean Technol. Environ. Policy 17 (2015) 1039–1051.

[10] N. Azouaou, Z. Sadaoui, A. Djaafri, H. Mokaddem, Adsorption of cadmium from aqueous solution onto untreated coffee grounds: Equilibrium, kinetics and thermodynamics, J. Hazard. Mater. 184 (2010) 126–134.

[11] M. Salman, M. Athar, U. Farooq, S. Rauf, U. Habiba, A new approach to modification of an agro-based raw material for Pb(II) adsorption, Korean J. Chem. Eng. 3 (2014) 467–474.

[12] A. Hashem, A.M. Azzeer, A. Ayoub, Removal of Hg (II) ions from laboratory wastewater onto phosphorylated haloxylonammodendron: Kinetic and equilibrium studies, Polym. Plast. Technol. Eng. 49 (2010) 1395–1404.

[13] A. Hashem, H.A. Hussein, M.A. Sanousy, E. Adam, E.E. Saad, Monomethylolatedthiourea—Sawdust as a new adsorbent for removal of Hg(II) from contaminated water, Equilibrium kinetic and thermodynamic studies, Polym. Plast. Technol. Eng. 50 (2011) 1220–1230.

[14] B.A. Fil, R. Boncukcuoğlu, A.E. Yilmaz, S. Bayar, Adsorption of Ni (II) on ion exchange resin: Kinetics, equilibrium and thermodynamic studies, Korean J. Chem. Eng. 29 (2012) 1232–1238.

[15] B.A. Fil, R. Boncukcuoglu, A.E. Yilmaz, S. Bayar, Adsorption kinetics and isotherms for the removal of Zinc Ions from aqueous solution by an ion-exchange resin, J. Chem. Soc. Pak. 34 (2012) 841–848.

[16] S.C. Tsai, K.W. Juang, Comparison of linear and non-linear forms of isotherm models for strontium sorption on a sodium bentonite, J. Radioanal. Nucl. Chem. 243 (2000) 741–746.

[17] G. Dual, R.M. Reinhardt, J.D. Reid, Carboxymethyl (CM) cottons prepared in non-aqueous media, Text. Res. J. 23 (1953) 719–726.

[18] A. Hashem, E.S. Abdel-Halim, Kh.F. El-Tahlawy, A. Hebeish, Enhancement of adsorption of Co (II) and Ni (II) ions onto peanut hulls though esterification using citric acid, Adsorpt. Sci. Technol. 23 (2005) 367–380.

[19] H.A. Elliot, C.P. Huang, The adsorption of Cu (II) complexes onto alumino sillicates, Water Res. 15 (1981) 849–855.

[20] A. Hashem, Amidoximated sunflower stalks as a new adsorbent for removal of Cu (II) from aqueous solution, Polym. Plast. Technol. Eng. 45 (2006) 35–42.

[21] H.C. Trivedi, V.M. Patel, R.D. Patel, Adsorption of cellulose triacetate on calcium silicate, Eur. Polym. J. 9 (1973) 525–531.

[22] Y.S. Ho, G. McKay, The kinetics of sorption of divalent metal ions onto sphagnum moss peat, Water Research 34 (2000) 735–742.
[23] W.J. Weber, J.C. Morris, Advances in water pollution research, Proc. 1st. Int. Conf. Water Pollut. Res. 2 (1962) 231–266.
[24] E. Tutem, R. Apak, C.F. Unal, Adsorptive removal of chlorophenols from water by bituminous shale, Water Res. 32 (1998) 2315–2324.
[25] S.H. Chien, W.R. Clayton, Application of Elovich equation to the kinetics of phosphate release and sorption in soils, Soil Sci. Soc. Am. J. 44 (1980) 265–268.
[26] Y.S. Ho, G. McKay, Sorption of dye from aqueous solution by peat, Chem. Eng. J. 70 (1998) 115–124.
[27] F.C. Wu, R.L. Tseng, R.S. Juang, Adsorption of dyes and phenols from water on the activated carbons prepared from corncob wastes, Environ. Technol. 22 (2001) 205–213.
[28] G. Annadurai, R.S. Juang, D.J. Lee, Use of cellulose-based wastes for adsorption of dyes from aqueous solutions, J. Hazard. Mater. 92 (2002) 263–274.
[29] V.J.P. Poots, G. McKay, J.J. Healy, Removal of basic dye from effluent using wood as an adsorbent, J. Water Pollut. Control Fed. 50 (1978) 926–935.
[30] K. Nagarethinam, M.S. Mariappan, Kinetics and mechanism of removal of methylene blue by adsorption on various carbons: A comparative study, Dyes Pigm. 51 (2001) 25–40.
[31] V.K. Gupta, Equilibrium uptake, sorption dynamics, process development and column operations for the removal of copper and nickel from aqueous solution and wastewater using activated slag: A low-cost adsorbent, Ind. Eng. Chem. Res. 37 (1998) 192–202.
[32] Z. Ding, R. Yu, X. Hu, Y. Chen, Adsorptive removal of Hg(II) ions from aqueous solutions using chemical-modified peanut hull powder, Pol. J. Environ. Stud. 23 (2014) 1115–1121.
[33] T.S. Anirudhan, L. Divya, M. Ramachandran, Mercury (II) removal from aqueous solutions and wastewaters using a novel cation exchanger derived from coconut coir pith and its recovery, J. Hazard. Mater. 157 (2008) 620–627.
[34] A. Ahmadpour, T.R. Bastami, M. Tahmasbi, M. Zabihi, Rapid removal of heavy metal ions from aqueous solutions by low cost adsorbents, Int. J. Global Environ Issues 12 (2012) 318–331.
[35] S.T. Song, N. Saman, K. Johari, H.B. Mat, Removal of mercury (II) from aqueous solution by using rice residues, J. Teknologi (Sci. Eng.) 63 (2013) 67–73.
[36] N.S. Labidi, Removal of mercury from aqueous solutions by waste brick, Int. J. Environ. Res. 2 (2008) 275–278.
[37] S. Basha, Z.V.P. Murthy, B. Jha, Sorption of Hg(II) from aqueous solutions onto Carica papaya: Application of isotherms, Ind. Eng. Chem. Res. 47 (2008) 980–986.
[38] R. Wahi, Z. Ngaini, V.U. Jok, Removal of mercury, lead and copper from aqueous solution by activated carbon of palm oil empty fruit bunch, World Appl. Sci. J. 5 (2009) 84–91.
[39] M.F. Yardim, T. Budinova, E. Ekinci, N. Petrov, M. Razvigorova, V. Minkova, Removal of mercury (II) from aqueous solution by activated carbon obtained from furfural, Chemosphere 52 (2003) 835–841.
[40] F.K. Onwu, C.U. Sonde, J.C. Igwe, Adsorption of Hg^{2+} and Ni^{2+} from aqueous solutions using unmodified and carboxymethylated granular activated carbon (Gac), Am. J. Phys. Chem. 6 (2014) 89–95.
[41] I. Langmuir, The constitution and fundamental properties of solids and liquids, JACS 38 (1916) 2221–2295.
[42] H. Freundlich, Over the adsorption in solution, J. Phys. Chem. 57 (1906) 385–470.
[43] M.J. Tempkin, V. Pyzhev, Kinetics of ammonia synthesis on promoted iron catalysts, Acta Phys. Chim. URSS 12 (1940) 217–222.
[44] M.M. Dubinin, Modern state of the theory of volume filling of micropore adsorbents during adsorption of gases and steams on carbon adsorbents, Zhurnal Fizicheskoi Khimii. 39 (1965) 1305–1317.
[45] G. Halsey, Physical adsorption on non-uniform surfaces, J. Chem. Phys. 16 (1948) 931–937.
[46] O. Redlich, D.L. Peterson, A useful adsorption isotherm, J. Phys. Chem. 63 (1959) 1024–1026.
[47] J. Toth, State equations of the solid gas interface layer, Acta Chem. Acad. Hung. 69 (1971) 311–317.
[48] R. Sips, Combined form of Langmuir and Freundlich equations, J. Chem. Phys. 16 (1948) 490–495.
[49] A.R. Khan, R. Ataullah, A. Al-Haddad, Equilibrium adsorption studies of some aromatic pollutants from dilute aqueous solutions on activated carbon at different temperatures, J. Colloid Interface Sci. 194 (1997) 154–165.
[50] C.J. Radke, J.M. Prausnitz, Adsorption of organic solutions from dilute aqueous solution on activated carbon, Ind. Eng. Chem. Fundam. 11 (1972) 445–451.
[51] R. Sips, On the structure of a catalyst surface, J. Chem. Phys. 16 (1948) 490–495.
[52] K.Y. Foo, B.H. Hameed, Insights into the modeling of adsorption isotherm systems, Chem. Eng. J. 156 (2010) 2–10.
[53] M. Baudu, Etude des interactions solute-fibres de charbonactif. Application et regeneration, Ph.D. Thesis, Universite de Rennes, Rennes, 1990.
[54] W. Fritz, E.U. Schlunder, Simultaneous adsorption equilibria of organic solutes in dilute aqueous solution on activated carbon, Chem. Eng. Sci. 29 (1974) 1279–1282.